ACADEMIA ROMÂNĂ
Revue Roumaine de Chimie
https://web.icf.ro/rrch/

Rev. Roum. Chim.,
2022, *67*(8–9), 473–482
DOI: 10.33224/rrch.2022.67.8-9.06

MATHEMATICAL MODEL OF ELECTROCATALYSIS OF METHANOL OXIDATION AT THE MIXTURE OF NANOCRYSTALS OF PLATINUM AND RUTHENIUM DIOXIDE

Milica SPASOJEVIĆ,[a,*] Dušan MARKOVIĆ[b] and Miroslav SPASOJEVIĆ[b]

[a]University of Belgrade, Innovative Centre of the Faculty of Chemistry, Studentski trg 12-16 Belgrade, Serbia
[b]University of Kragujevac, Faculty of Technical Sciences, Joint Laboratory for Advanced Materials of SASA, Section for Amorphous Systems, Svetog Save 65 Čačak, Serbia

Received April 14, 2022

Mathematical model representing a catalytic effect of a nanocrystal mixture of metallic platinum and ruthenium dioxide for electrooxidation of methanol is established. Dependance of a current density of the methanol electrooxidation on the chemical composition and size of nanocrystals is determined in the model. A good agreement between theoretical values and experimental results corroborates that electrooxidation of methanol is guided by a bifunctional mechanism. The model is based on the fact that the catalytic effect is proportional to the length of the contact border between nanocrystals of metallic platinum and nanocrystals of ruthenium dioxide. Ru-OH particles are formed on the Ru atoms at the border of crystal grains, at potentials more negative than on platinum. These species oxidize firmly bound intermediates CO_{ad} located on the adjacent Pt atoms and thus release the Pt atoms for adsorption and dehydrogenation of subsequent molecules of methanol.

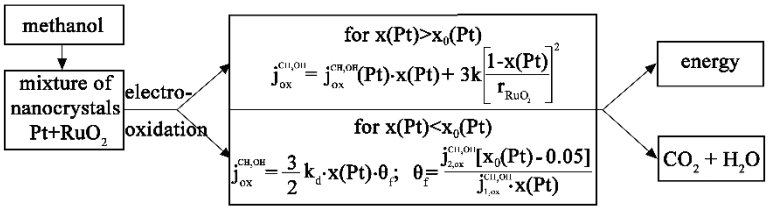

INTRODUCTION

In the last couple of decades, research of many scientific groups has been focused on development of renewable energies, i.e. fuel cells, particularly direct liquid-feed fuel cells. The use of hydrogen in fuel cells is unfavorable due to high costs of miniaturized storage containers and potential danger during its application and transportation. Additionally, low gas-phase energy density of hydrogen also limits its use in fuel cells.[1] Thus, major research studies have been targeted towards finding an appropriate replacement for hydrogen. To this end, hydrogen was substituted with small organic molecules, such as methanol, formaldehyde, formic acid, 1- and 2-propanol in the liquid fuel cells. Unlike gaseous cells, the liquid fuel cells have a high theoretical energy density (~ 9 kWh kg^{-1}) and are easy to handle, transport and distribute.[2] Therefore, a lot of efforts have been put into development of direct simple organic molecules fuel cells as potential power sources for portable electronic devices (mobile phones, lap tops, digital cameras etc.).[3,4]

Oxidation of simple organic molecules begins with their adsorption on the surface of the most investigated catalyst, Pt. Then, the adsorbed organic molecules are subjected to dehydrogenization, thus producing different intermediates. These intermediates can be strongly and weakly adsorbed.[2, 5–21] The CO_{ad} species are strongly

* Corresponding author: smilica84@gmail.com

adsorbed on the surface of the most effective catalyst, Pt.[2, 5–25] Besides CO_{ad}, strongly adsorbed COH_{ad} species, which block the surface of Pt and prevent further oxidation of subsequent organic molecules, are also formed.[22–25] Hence, the Pt catalyst shows a low activity towards the electrooxidation of small organic molecules. Due to high costs and low durability, extensive studies have been done on platinum-based electrocatalysts (Pt/Sn, Pt/Ti, Pt/Mn, Pt/Co, Pt/Fe, Pt/Bi, Pt/NI, Pt/Ru and Pt/RuO_2) for fuel cell applications.[5-8, 24–50] The research conducted in last three decades showed the best catalytic performance of Pt/Ru and Pt/RuO_2 catalysts in the particular application.[5–8, 24, 25, 32–41] The catalytic effect of these catalysts was attributed to both bifunctional mechanism and electronic effect. The leading effect was the bifunctional mechanism, in which the oxy species were formed on Ru atoms at more negative potentials than on Pt atoms. These oxy species strongly oxidize some weakly adsorbed intermediates, bound to adjacent Pt atoms, releasing the Pt atoms and allowing for dehydrogenation of the subsequent organic molecules.[5–8, 24, 25, 32–41] The electronic effect is caused by shifting of the d-band center of Pt in Pt/Ru alloys away from the Fermi level.[32, 33, 36, 41, 51–54] M. Wakisaka *et al.* have studied electronic structures of pure Pt and P/Ru alloy electrodes by combining XPS with an electrochemical cell.[51] They have shown that alloying with Ru caused the positive shift of $Pt4f_{7/2}$. A linear relationship between the core level shifts and the CO adsorption energy and thus, weaker adsorption of CO on Pt/Ru have been found. P. Waszeruk *et al.* and C. Lui *et al.* have determined a definite contribution of the electronic effect to the total enhancement of CO_{ad} oxidation on Pt/Ru as compared to pure Pt, which was only one-fourth of that of the bifunctional mechanism.[53, 54] M.A. Rigsby *et al.* have examined the effect of the electronic structure of Pt/Ru alloy nanoparticles on reactivity of small organic molecules by combining synchrotron radiation photoelectron spectroscopy and electrochemistry.[52] They have found a linear increase in Pt core-level binding energies with addition of Ru. This behavior was attributed to the lattice strain and charge transfer. Also, it has been found that the bifunctional mechanism contributed more significantly than the electronic effect. R. D. Rolison *et al.* have discovered that hydrous Pt/Ru catalysts were more efficient than Pt/Ru alloys, indicating the significance of Ru-OH species in the mechanism of methanol oxidation.[55, 56] R. P. L. Profeti *et al.* have synthetized unform films $Pt_xRu_{(1-x)}O_y$ with controlled stoichiometry, a high surface area, good chemical stability and uniform composition throughout the film by thermal decomposition of polymeric precursors. The highest catalytic activity was obtained with the catalyst $Pt_{0.6}Ru_{0.4}O_y$. The catalytic effect of the $Pt_xRu_{(1-x)}O_y$ catalysts on methanol oxidation was a result of the existence of amorphous and hydrated RuO_2 and its ability to donate OH species. These OH species promoted the oxidation of CO_{ad} to CO_2. A. A. Belmesov *et al.* have applied Pt particles of the average size of 5 to 7 nm on the $Ti_{(1-x)}Ru_xO_{2-\delta}$ support.[47] The tolerance of the catalyst towards CO has been found to be dependable on the crystal structure of the support. A higher rate of CO oxidation was obtained with the support with the rutile structure than the support with the anatase structure. When using the catalysts Pt/ $Ti_{(1-x)}Ru_xO_{2-\delta}$ with supports with both rutile and anatase structures, the potential of the onset of CO oxidation decreased with increasing the concentration of RuO_2.

M. Spasojevic *et al.* have prepared the catalytic coating composed of the mixture of nanocrystals of metallic Pt and RuO_2 of the rutile structure by the thermal procedure on a Ti substrate and used it for the oxidation of CH_3OH, CH_2O, HCOOH, CH_3-CH_2-CH_2OH and CH_3-CHOH-CH_3.[24, 25, 37–40] It has been found that an increase in the RuO_2 content resulted in the increase in the catalytic activity up to maximum value and its subsequent decrease. The organic molecule oxidation on the coatings with the RuO_2 content higher than optimal was determined by dehydrogenation, whereas the oxidation of strongly bound intermediates, CO_{ad}, with oxy species adsorbed on Ru atoms determined the organic molecules oxidation on the coatings with the RuO_2 content lower than optimal. The catalytic effect was a result of the bifunctional mechanism, in which the oxy species were formed on Ru in the rutile structure of RuO_2 at more negative potentials than on pure platinum. These oxy species oxidized intermediates firmly and weakly adsorbed on ensembles of few adjacent Pt atoms at the metallic nanocrystals surface.

This study is aimed to create a mathematical model to predict the catalytic effect of the mixture of nanocrystals of metallic Pt and RuO_2 of rutile structure on the electrooxidation of methanol. The mathematical model is used to determine the nature of catalytic effect, which would allow for designing the optimal chemical composition and microstruc-

ture of Pt/RuO_2 catalyst for the oxidation of simple organic molecules.

RESULTS AND DISCUSSION

The thermal procedure is used to form an active catalytic coating, composed of the mixture of nanocrystals of metallic Pt and RuO_2 of the rutile structure, on the titanium substrate, applied in electrochemical oxidation of small organic molecules.[24, 25, 37–40] M. Spasojevic *et al.* have determined the effect of both the mean crystals size and experimental coating composition on the nominal coating composition using the XRD analysis, as shown in Fig. 1.[38]

With increasing the RuO_2 content in the active mixture, the mean crystal size of RuO_2 increases, whereas the mean crystal size of Pt decreases.[38] Experimental molar percentages of Pt are always somewhat lower than nominal. This difference is more pronounced at higher contents of Pt in the solution, applied on the Ti substrate. Previous research have shown that the RuO_2 content affected the catalytic activity of the coating in the electrooxidation of CH_3OH, CH_2O, HCOOH, CH_3-CH_2-CH_2OH and CH_3-CHOH-CH_3.[24, 37–40] With increasing the RuO_2 content, the catalytic activity increased, reached its maximum and then decreased. The catalytic effect of the mixture of nanocrystals of metallic Pt and RuO_2 of the rutile structure has been attributed to the bifunctional mechanism.[24, 37–40] In order to corroborate the bifunctional mechanism, a mathematical model of the catalytic effect of the mixture of nanocrystals of Pt and RuO_2 on the methanol oxidation is set.

The overall oxidation of methanol in acid fuel cells is a 6-electron process which proceeds as follows:

$$CH_3OH + H_2O \rightarrow CO_2 + 6H^+ + 6e \qquad E^0 = 0.02\ V;\ pH = 0. \tag{1}$$

Electrooxidation of CH_3OH is a multi-step process. Prior to CO_{ad} development at the electrode, there are four consecutive single-electron stages:

$$CH_3OH + Pt \rightarrow Pt\text{-}CO_{ad} + 4H^+ + 4e \tag{2}$$

Then CO_{ad} is oxidized by the oxy species formed on Pt or Ru:

$$Pt(Ru) + H_2O \rightarrow Pt(Ru)\text{-}OH + H^+ + e \tag{3}$$

$$Pt\text{-}CO_{ad} + Pt\text{-}OH \rightarrow 2Pt + CO_2 + H^+ + e \tag{4}$$

The oxy species formed on Ru at more negative potentials than on Pt, oxidize adsorbed CO_{ad} on the adjacent Pt atoms at more negative potentials.

$$Ru\text{-}OH + Pt\text{-}CO_{ad} \rightarrow Ru + Pt + CO_2 + H^+ + e \tag{5}$$

The released Ru atoms can react with new OH species arriving from adjacent Ru atoms by surface diffusion, or the discharged Ru atoms can participate in reaction (2) and form new OH_{ad} species.

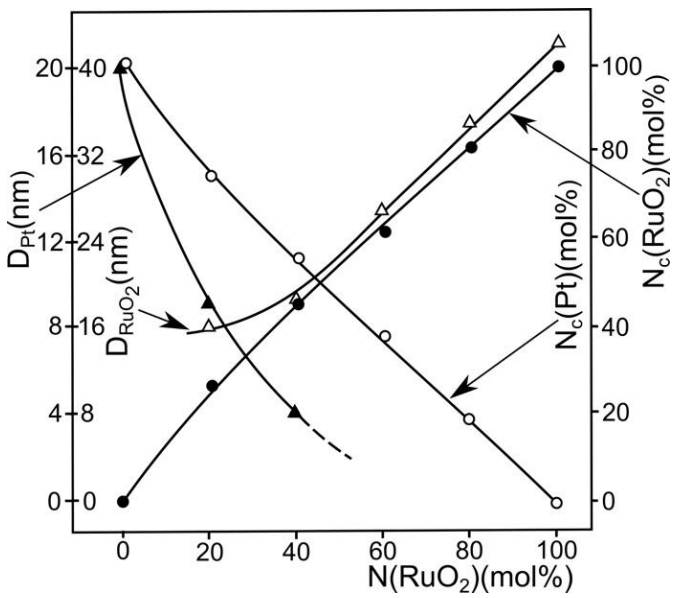

Fig. 1 – The content of (○) Pt (Nc(Pt)), and (●) RuO_2 (Nc(RuO_2)) in the coating and the mean crystals size of (▲) Pt (D(Pt)) and (△) RuO_2 (D(RuO_2)) as a function of the nominal coating composition, N(RuO_2).

Simultaneously, at released Pt atoms CO_{ad} species are reformed by dehydrogenation of CH_3OH or by coming of new CO species from adjacent Pt atoms by rapid diffusion.

Reactions (1)–(4) compose a main reaction pathway of CH_3OH oxidation. However, side reactions also occur simultaneously with the main pathway. The rates of these side reactions are negligible compared to the rate of the main reaction pathway.[24, 25, 37–40]

The following assumptions are made prior to setting the mathematical model:

1. The catalytic effect is a result of CO_{ad} oxidation on Pt atoms with Ru-OH species located on the contact edge of RuO_2 nanocrystals.[24, 25, 37–40]
2. Surface diffusion of the firmly bound intermediates CO_{ad} over the surface of Pt nanocrystals to the grain border is a rapid process.[57]
3. Diffusion of OH species over the surface of RuO_2 nanocrystals to Ru atoms at the grain border and reaction of RuOH species formation from H_2O molecules are rapid processes.[24, 25, 37–40, 57–59]

These assumptions indicate the increase in the rate of oxidation of the firmly bound intermediate CO_{ad} with rising the size of the contact border between nanocrystals of Pt and RuO_2. The increase in the contact border results in rise in the rate of methanol oxidation until the rates of dehydrogenation and CO_{ad} oxidation equalize. After the rates equalization, the increase in the RuO_2 content declines the catalytic effect due to lower number of ensembles of Pt atoms, required for adsorption and dehydrogenation of CH_3OH.

When the content of RuO_2 is lower than that of Pt, it can be assumed that the RuO_2 nanocrystals are completely surrounded by the Pt nanocrystals. The contact border length between the nanocrystals of Pt and RuO_2 is equal to that of RuO_2 nanocrystals. It is assumed that the average surface of nanocrystals is of circular shape and the radius of the average size of RuO_2 nanocrystals, r_{RuO_2} is approximately equal to ½ D_{RuO_2}. The length of the contact border of one RuO_2 nanocrystal, surrounded by the Pt nanocrystals is:

$$l = 2 \cdot r_{RuO_2} \pi \tag{6}$$

where: l – perimeter of RuO_2 nanocrystal and r_{RuO_2} – radius of the average size of RuO_2 nanocrystals.

The number of RuO_2 species, n_{RuO_2}, at the real surface of an electrode is determined by the equation:

$$n_{RuO_2} = \frac{S \cdot (1 - x(Pt))}{r_{RuO_2}^2 \pi} \tag{7}$$

where: n_{RuO_2} – the number of RuO_2 nanocrystals at the real surface of the electrode, S – the real surface of the electrode and x = 0.01Nc(Pt) – moll fraction of the Pt in the coating. The total length of the contact edges, L, between Pt and RuO_2 nanocrystals is:

$$L_{Ru} = n_{RuO_2} \cdot 2 r_{RuO_2} \pi = \frac{2 \cdot S \cdot (1 - x(Pt))}{r_{RuO_2}} \tag{8}$$

The real surface is determined by the equation:

$$S = S_G \cdot F_R \tag{9}$$

where: S_G – geometric surface area, F_R – roughness factor. The roughness factor used in this paper is independent of the chemical composition.[38]

At higher Pt contents, the slowest step in the oxidation of small organic molecules is the reaction of oxidation of firmly bound intermediates with adsorbed OH species. The total current density of the oxidation of CO_{ad}, $j_{u,ox}^{CO}$, is determined by the following equation:

$$j_{u,ox}^{CO} = j_{ox}^{CO}(Pt) \cdot x(Pt) + j_{ox}^{CO}(Pt/RuO_2) \tag{10}$$

where: $j_{u,ox}^{CO}$ – the total current density of CO_{ad} oxidation, : $j_{ox}^{CO}(Pt)$ – the current density of oxidation at pure Pt, $j_{ox}^{CO}(Pt/RuO_2)$ – the current density of oxidation caused by the catalytic effect of the nanocrystals mixture.

With increasing the size of the contact border, the number of RuOH species and firmly adsorbed intermediates rises linearly at that border, thus:

$$j_{ox}^{CO}(Pt/RuO_2) = k_{ox}^{Pt/RuO_2} \cdot c(RuOH) \cdot c(CO) \cdot 4 \cdot F_R \left[\frac{(1 - x(Pt))}{r_{RuO_2}}\right]^2 \tag{11}$$

where: k_{ox}^{Pt/RuO_2} – the rate constant of the reaction (11), c(RuOH) – the linear concentration of the RuOH species at the contact border and c(CO) – the linear concentration of the CO_{ad} intermediate at the contact border. The linear concentration of RuOH is proportional to the degree of coverage of Ru atoms with OH species:

$$c(RuOH) = k(RuOH) \cdot \theta(RuOH) \tag{12}$$

The reaction of RuOH formation (3) and surface diffusion of the OH_{ad} species over RuO_2 crystals to their edge are substantially more rapid processes than reaction (5).[24,25,37–40,57–59] Therefore, θ(RuOH) and c(RuOH) are constants at the given potential. Thus:

$$c(RuOH) = k'(RuOH) \tag{13}$$

where:

$$k'(RuOH) = k(RuOH) \cdot \theta(RuOH) \tag{14}$$

The linear concentration of the intermediate CO_{ad} at the contact borders of Pt nanocrystals is proportional to the coverage degree of the Pt surface with CO_{ad}:

$$c(CO_{ad}) = k(CO) \cdot \theta(CO_{ad}) \tag{15}$$

when both reaction of CH_3OH dehydrogenation and the surface diffusion of CO_{ad} over the Pt crystals are more rapid processes than the oxidation of the intermediate CO_{ad}, then $\theta(CO_{ad})$ and $c(CO_{ad})$ are constants at given potential.[24,25,37-40,57–59] Therefore:

$$c(CO_{ad}) = k'(CO) \tag{16}$$

where:

$$k'(CO) = k(CO) \cdot \theta(CO_{ad}) \tag{17}$$

By introducing a new constant k, determined by the equation:

$$k = 4 \cdot F_R \, k_{ox}^{Pt/RuO_2} \cdot k'(RuOH) \cdot k'(CO) \tag{18}$$

the total current density of CO_{ad} oxidation is expressed as:

$$j_{u,ox}^{CO} = j_{ox}^{CO}(Pt) \cdot x(Pt) + k \cdot \left[\frac{1-x(Pt)}{r_{RuO_2}}\right]^2 \tag{19}$$

From equations (1)-(5), the current density of CH_3OH oxidation is:

$$j_{ox}^{CH_3OH} = j_{u,d}^{CH_3OH} + j_{u,ox}^{CO} \tag{20}$$

and:

$$j_{u,d}^{CH_3OH} = 2 \cdot j_{u,ox}^{CO} \tag{21}$$

where: $j_{ox}^{CH_3OH}$ – the current density of CH_3OH oxidation and $j_{u,d}^{CH_3OH}$ – the total current density of dehydrogenation.

The equation for the current density of oxidation is obtained by combining equations (19), (20) and (21):

$$j_{ox}^{CH_3OH} = j_{ox}^{CH_3OH}(Pt) \cdot x(Pt) + 3 \cdot k \left[\frac{1-x(Pt)}{r_{RuO_2}}\right]^2 \tag{22}$$

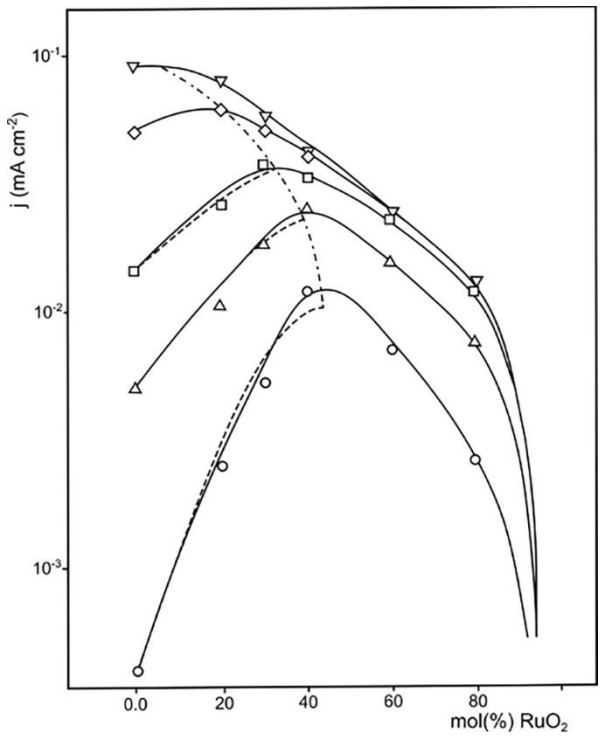

Fig. 2 – The current density of CH_3OH oxidation as a function of the content and coating potentials. Experimental values: (○) 0.517 V; (△) 0.550 V; (□) 0.583 V; (◇) 0.633 V; (▽) 0.667 V. The current density values were recorded after holding the anode for 3 min at 0.049 V and 30 min at desired potential (solution: 0.5 mol dm^{-3} H_2SO_4 + 0.25 mol dm^{-3} CH_3OH; t = 25 °C). The curves presented with dashed lines are obtained from the equation (22). The dash-dotted curve presents dependence of the maximum of current density on potential.

Fig. 2 shows dependance of the current density of CH_3OH oxidation on the potential and active coating content, obtained either experimentally or theoretically by applying equation (22).

Fig. 1 shows that the increase in the RuO_2 content results in rise in the catalytic activity, which reaches the maximum value at a certain composition of the coating. Subsequent increase of the RuO_2 content declines the catalytic activity. At the RuO_2 contents lower than maximal, the rate of methanol oxidation is determined by the slow reaction of oxidation of the firmly bound intermediate CO_{ad}. With increasing the RuO_2 content, the oxidation of CO_{ad} accelerates (reaction (5)) due to increase in the length of the contact edge between nanocrystals of Pt and RuO_2. Simultaneously, the rate of CH_3OH dehydrogenation (reaction (2)) declines as a result of decrease in the surface of Pt nanocrystals and hence, the number of ensembles of adjacent Pt atoms. At the certain RuO_2 concentration, when rates of these two reactions equalize, the maximum catalytic effect of the coating is accomplished.[38] As shown in Fig. 2, with decreasing the potential below 0.67 V, the RuO_2 content shifts to the higher values for the maximum catalytic activity of the coating. At the coatings with more than the optimal amount of RuO_2, the rate of methanol oxidation is determined by the CH_3OH dehydrogenation. A high coverage degree of Ru atoms with oxy species, which are formed at more negative potentials than on Pt, results in more comprehensive oxidation of CO_{ad} on the Pt/RuO_2 coating at potentials more negative than 0.67 V than on pure Pt.[25, 38] As a consequence, the coverage degree of Pt atoms of the active coating with the firmly adsorbed CO_{ad} species rapidly declines at more negative potentials than on pure Pt.[25, 38]

By fitting the equation (22) with experimentally obtained dependances, shown in Fig. 1, the values of the constant k at different potentials are determined. Subsequently, these values and experimental results from Fig. 1 are used to calculate the theoretical values of $j_{ox}^{CH_3OH}$. Good agreement between the theoretically obtained and experimental values (Fig. 2) indicates validity of the proposed mechanism of the CH_3OH electrooxidation on the mixture of nanocrystals of Pt and RuO_2, at the RuO_2 contents lower than optimal.

When the RuO_2 contents are greater than optimal, the current density of oxidation is determined by the reaction of dehydrogenation of CH_3OH (reaction 2):

$$j_{ox}^{CH_3OH} = \frac{3}{2} \cdot j_{u,d}^{CH_3OH} \tag{23}$$

The total current density of dehydrogenation is proportional to the molar fraction of Pt and its fraction of free surface area θ_f:

$$j_{u,d}^{CH_3OH} = k_d \cdot x(Pt) \cdot \theta_f = k_d \cdot x(Pt) \cdot \left(1 - \theta(CO_{ad})\right) \tag{24}$$

According to the proposed mechanism, the coverage degree $\theta(CO_{ad})$ is negligible for the electrode with the Pt content 5 mol% lower than the optimal $[x_0(Pt) - 0.05]$, and thus:

$$j_{1,u,d}^{CH_3OH} = k_d \cdot [x_0(Pt) - 0.05] \tag{25}$$

At the same potential, the total current density of dehydrogenation, $j_{2,u,d}^{CH_3OH}$, on the coating with $x(Pt) < x_0(Pt) - 0.05$ is:

$$j_{2,u,d}^{CH_3OH} = k_d \cdot x(Pt) \cdot \theta_f \tag{26}$$

Combination of the equation (23), (25) and (26) results in:

$$\theta_f = \frac{j_{2,u,d}^{CH_3OH} \cdot [x_0(Pt) - 0.05]}{j_{1,u,d}^{CH_3OH} \cdot x(Pt)} = \frac{j_{2,ox}^{CH_3OH} \cdot [x_0(Pt) - 0.05]}{j_{1,ox}^{CH_3OH} \cdot x(Pt)} \tag{27}$$

Using the equation (27) and the experimental data shown in Fig. 2, dependance of θ_f on the RuO_2 content and potential is obtained (Fig. 3). As seen in Fig. 3, $\theta_f \approx 1$ in the RuO_2 content region from optimal to x(RuO_2) = 0.45. From x(RuO_2) = 0.45 to x(RuO_2) = 0.81, θ_f slowly decreases till $\theta_f = 0.75$. The change in the RuO_2 content from optimal to x(RuO_2) = 0.40 results in decrease in the average size of Pt nanocrystals to 4 nm (Fig. 1). When Pt nanocrystals are larger than 4 nm, the number of ensembles of adjacent Pt atoms, required for the CH_3OH adsorption, is proportional to the Pt surface. Therefore, θ_f stays constant in this region of the RuO_2 contents. However, the increase in the RuO_2 content from x(RuO_2) = 0.45 to x(RuO_2) = 0.81 results in decline in the average size of nanocrystals to values below 3 nm (Fig. 1). This causes the decrease in the number of ensembles of adjacent Pt atoms, required for the CH_3OH adsorption, per the surface unit of Pt, resulting in drop of the current density of CH_3OH dehydrogenation and thus θ_f.[60] Therefore, θ_f decreases as a consequence of the increased number of Pt atoms at edges and stairs that cannot be included into ensembles of Pt atoms, which adsorb CH_3OH molecules.[60]

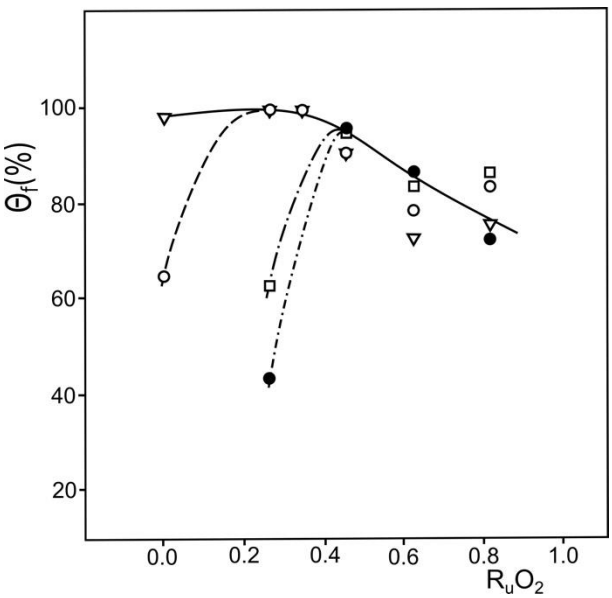

Fig. 3 – θ_f as a function of the RuO_2 content and potential: (▽) 0.667 V; (○) 0.633 V; (□) 0.550 V; (●) 0.517 V (solution: 0.5 mol dm^{-3} H_2SO_4 + 0.25 mol dm^{-3} CH_3OH; t = 25 °C).

In the region of RuO_2 contents that are below the optimal value, with decreasing the RuO_2 content θ_f declines (Fig. 3). Here, as a consequence of the decrease in the RuO_2 content, difference between the rates of CH_3OH dehydrogenation and CO_{ad} oxidation rises, resulting in the increase in the coverage degree of Pt with CO_{ad} and thus, the decline in θ_f. The presented figures and theoretical considerations indicate the validity of the proposed mechanism of the catalytic effect of the mixture of Pt and RuO_2 nanocrystals in the electrooxidation of CH_3OH. Insight in the mechanism of electrocatalytical oxidation of small organic molecules would allow for determination of the optimal composition and microstructure of the Pt/RuO_2 catalyst and thus, the parameters of its synthesis.

EXPERIMENTAL

An active coating composed of the mixture of nanocrystals of metallic Pt and RuO_2 of the rutile structure on a titanium substrate of a surface area of 3.0 cm^2, was prepared by the thermal procedure previously described.[38] Briefly, the solutions H_2PtCl_6 and $RuCl_3$ (Johnson and Matthey) in 2-propanol were spread over the properly prepared surface of titanium plates. After evaporation of the solvent, the titanium plates were heated for 5 minutes at 500 °C in the air atmosphere. The procedure was repeated five times until the coating depth of 1.2 mgcm^{-2} based on the pure metals was achieved. After spreading of the last layer, the electrodes were heated for 45 minutes at 500 °C.

The chemical composition of the layer was determined by electronic dispersion spectroscopy, EDS (QX3000 spectrometer).

A Phillips PW1730 diffractometer with a vertical goniometer PW 1050 and a static non-rotating sample carrier was used for X-ray diffraction analyses. This had a 35 kV, 20 mA power supply for copper excitation, and an AMR graphite monochromator. Phases were identified by reference to ASTM tables.

The electrochemical measurements were carried out with the usual electrical set-up consisting of a potentiostat equipped with a programmer (Potentiostat-Galvanostat model 173, EGG Princeton, Applied Research, Princeton, USA), an x-y recorder (Hewlett Packard 7035 B) and a digital voltmeter (Pros´Kit 03-9303 C). The experiments were conducted in a standard electrochemical cell with a separate part for the saturated mercury sulphate electrode and Luggin capillary. The counter electrode was a flat platinum mesh with a geometric surface area of 16 cm^2 placed parallel to the working electrode. The cell was placed in the thermostat. The operating temperature was 25±0.5 °C. The solutions were made from p.a. chemicals (Merc) and demineralized water. Prior to the electrochemical measurements, oxygen was removed from the solution by the introduction of nitrogen that was firstly purified by passing over molecular sieves and copper shavings. All potentials were expressed relative to the standard hydrogen electrode. The potentials were corrected for the ohmic potential drop, which was determined by the galvanostatic pulse method. The current density values were recorded after holding the electrode for 3.0 min at 0.049 V and 30.0 min at desired potential. When the electrode was kept at desired potential, the initial value of current decreases instantly to substantially lower value after 30.0 min, and remains approximately constant following 60 min.

CONCLUSIONS

In this paper, the mathematical model of the effect of the chemical composition of the Pt/RuO_2 coating on its catalytic activity in the electrooxidation of methanol is set. The coating is formed by the thermal procedure and composed of the mixture of

nanocrystals of metallic Pt and RuO_2 of the rutile structure. The correlation between the chemical composition and size of nanocrystals as well as the current density of electrooxidation of methanol at different potentials is established. Good agreement between experimental and theoretical values indicates the validity of the proposed bifunctional mechanism in catalyze of the methanol electrooxidation reaction. The mathematical model shows that the increase in the RuO_2 content causes the rise in the catalytic activity up to the maximum value and then its decrease. This model corroborates that the increase in the catalytic activity with rising the RuO_2 content up to optimal value is caused by the increase in the length of a contact border between nanocrystals of metallic Pt and RuO_2. Ru-OH species are formed on the Ru atoms at the border of nanocrystals, at potentials more negative than on metallic Pt. These oxy species oxidize firmly bound intermediates CO_{ad}, located on adjacent Pt atoms and thus, release these Pt atoms for adsorption and dehydrogenation of subsequent CH_3OH molecules. When the RuO_2 content is higher than optimal, the catalytic activity is determined by the reaction of methanol dehydrogenation. In this region, the increase in the RuO_2 content results in decline of the catalytic activity due to the decrease in the Pt surface and thus, the number of ensembles of adjacent Pt atoms required of the methanol adsorption.

Acknowledgments. This work was funded by the Ministry of Education, Science and Technological Development of the Republic of Serbia [Project Ref. No. 170257 and Grant No. 451-03-68/2022-14/200288, Innovative Centre of the Faculty of Chemistry, University of Belgrade].

Nomenclature list

1. $N_c(Pt)$, mol% – content of Pt in the coating
2. $N_c(RuO_2)$, mol% – content of RuO_2 in the coating
3. $N(Pt)$, mol% – nominal content of Pt in the coating
4. $N(RuO_2)$, mol% – nominal content of RuO_2 in the coating
5. $D(Pt)$, nm – mean crystal size of Pt
6. $D(RuO_2)$, nm – mean crystal size of RuO_2
7. E^{θ}, V – standard electrode potential
8. r_{RuO_2}, nm – radius of average crystal size of RuO_2
9. r_{Pt}, nm – radius of average crystal size of Pt
10. $x(Pt)$ – mol fraction of Pt in the coating
11. S, cm^2 – real surface area
12. L, nm – total length of the contact edge between Pt and RuO_2 nanocrystals
13. S_G, cm^2 – geometric surface area
14. F_R – friction factor
15. $j_{u,ox}^{CO}$, mA cm^{-2} – total current density of the CO_{ad} oxidation
16. $j_{ox}^{CO}(Pt)$, mA cm^{-2} – current density of the CO_{ad} oxidation at pure Pt
17. $j_{ox}^{CO}(Pt/RuO_2)$, mA cm^{-2} – current density of the oxidation caused by the catalytic effect of the nanocrystals mixture
18. k_{ox}^{Pt/RuO_2}, mA cm^2 mol^{-2} – rate constant of the oxidation reaction caused by the catalytic effect of the nanocrystals mixture
19. $c(RuOH)$, mol cm^{-1} – linear concentration of RuOH at the constant border between nanocrystals Pt and RuO_2
20. $\theta(RuOH)$ – coverage degree of Ru with OH_{ad} species
21. $k(RuOH)$, mol cm^{-1} – constant of proportionality between $c(RuOH)$ and $\theta(RuOH)$ in the equation (12)
22. $k'(RuOH)$, mol cm^{-1} – constant in the equation (14)
23. $c(CO_{ad})$, mol cm^{-1} – linear concentration of CO_{ad} at the contact border between nanocrystals Pt and RuO_2
24. $k(CO)$, mol cm^{-1} – constant of proportionality between $c(CO_{ad})$ and $\theta(CO_{ad})$ in the equation (15)
25. $\theta(CO_{ad})$ – coverage degree of Pt with CO_{ad} species
26. $k'(CO)$, mol cm^{-1} – constant in the equation (17)
27. k, mA – constant in the equation (18)
28. $j_{ox}^{CH_3OH}$, mA cm^{-2} – current density of the CH_3OH oxidation
29. $j_{ox}^{CH_3OH}$, mA cm^{-2} – current density of the CH_3OH oxidation at pure Pt
30. $j_{u,d}^{CH_3OH}$, mA cm^{-2} – total current density of the CH_3OH dehydrogenation
31. θ_f – fraction of the free Pt surface
32. k_d, mA cm^{-2} – rate constant of the CH_3OH dehydrogenation
33. $x_0(Pt)$ – optimal mol fraction of Pt
34. $j_{1,u,d}^{CH_3OH}$, mA cm^{-2} – total current density of the CH_3OH dehydrogenation at the coating surface with the composition of $x_0(Pt)$ – 0.05
35. $j_{2,u,d}^{CH_3OH}$, mA cm^{-2} – total current density of the CH_3OH dehydrogenation at the coating surface with the composition of $x(Pt)<x_0(Pt)$ – 0.05

36. $j_{1,ox}^{CH_3OH}$, mA cm^{-2} – current density of the CH_3OH oxidation at the coating surface with the composition of $x_0(Pt)$ – 0.05
37. $j_{2,ox}^{CH_3OH}$, mA cm^{-2} – current density of the CH_3OH oxidation at the coating surface with the composition of $x(Pt)<x_0(Pt)$ – 0.05.

REFERENCES

1. Yu and P.G. Pickup, *J. Power Sources*, **2008**, *182*, 124–132.
2. M. Nacef, M. L. Chelaghmia, A. M. Affoune and M. Pontié, *Materials Research Foundations*, **2019**, *49*, 103–128.
3. V. M. Barragán and A. Heinzel, *J. Power Sources*, **2002**, *104*, 66–72.
4. H. Tang, S. Wang, M. Pan, S. P. Jiang and Y. Ruan, *Electrochim. Acta*, **2007**, *52*, 3714–3718.
5. H. Liu, C. Song, L. Zhang, J. Zhang, H. Wang and D. P. Wilkinson, *J. Power Sources*, **2006**, *155*, 95–110.
6. X. Zhao, M. Yin, L. Ma, L. Liang, C. Liu, J. Liao, T. Luc and W. Xing, *Energy Environ. Sci.*, **2011**, *4*, 2736–2753.
7. N. Kakati, J. Maiti, S. H. Lee, S. H. Jee, B. Viswanathan and Y. S. Yoon, *Chem. Rev.*, **2014**, *114*, 12397–12429.
8. A. Heinzel and V. M. Barragán, *J. Power Sources*, **1999**, *84*, 70–74.
9. O. A. Petrii, *Russ. J. Electrochem*., **2019**, *55*, 1–33.
10. O. A. Petrii, *J. Solid State Electrochem.*, **2008**, *12*, 609.
11. T. H. M. Housmans, A. H. Wonders and M. T. M. Koper, *J. Phys. Chem. B*, **2006**, *110*, 10021–10031.
12. J. Schnaidt, Z. Jusys, R. J. Behm, *J. Phys. Chem. C*, **2012**, *116*, 25852–25867.
13. Z. D. Wei, L. L. Li, Y. H. Luo, C. Yan, C. X. Sun, G. Z. Yin and P. K. Shen, *J. Phys. Chem. B*, **2006**, *110*, 26055–26061.
14. J. W. Guo, T. S. Zhao, J. Prabhuram, R. Chen and C. W. Wong, *J. Power Sources*, **2006**, *156*, 345–354.
15. J. Schnaidt, M. Heinen, Z. Jusys and R. J. Behm, *Electrochim. Acta*, **2013**, *104*, 505–517.
16. E. Pastor, S. Wasmus, T. Iwasita, M. C. Arévalo, S. González and A. J. Arvia, *J. Electroanal. Chem.*, **1993**, *350*, 97–116.
17. P. Olivi, L. O. S. Bulhões, J.-M. Léger, F. Hahn, B. Beden and C. Lamy, *J. Electroanal. Chem*., **1994**, *370*, 241–249.
18. P. Olivi, L. O. S. Bulhões, J.-M. Léger, F. Hahn, B. Beden and C. Lamy, *Electrochim. Acta*, **1996**, *41*, 927–932.
19. M. T. M. Koper, M. Hachkar and B. Beden, *J. Chem. Soc., Faraday Trans.*, **1996**, *92*, 3975–3982.
20. A. Miki, S. Ye, T. Senzaki and M. Osawa, *J. Electroanal. Chem.*, **2004**, *563*, 23–31.
21. G. Samjeské, A. Miki and M. Osawa, *J. Phys. Chem. C*, **2007**, *111*, 15074–15083.
22. M. D. Spasojević, R. R. Adić and A. R. Despić, *J. Electroanal. Chem.*, **1980**, *109*, 261–269.
23. R. R. Adžić, M. I. Hofman and D. M. Dražić, *J. Electroanal. Chem.*, **1980**, *110*, 361–368.
24. M. Spasojevic, M. Spasojevic and L. Ribic-Zelenovic, *Monatsh. Chem.*, **2020**, *151*, 33–43.
25. M. Spasojević, L. Ribic-Zelenović, M. Spasojević and T. Trišović, *Rev. Roum. Chim.*, **2020**, *65*, 481–489.
26. D. Y. DeSario and F. J. DiSalvo, *Chem. Mater.*, **2014**, *26*, 2750–2757.
27. Z. Cui, H. Chen, M. Zhao, D. Marshall, Y. Yu, H. Abruña and F. J. DiSalvo, *J. Am. Chem. Soc.*, **2014**, *136*, 10206–10209.
28. T. Ghosh, B. M. Leonard, Q. Zhou and F. J. DiSalvo, *Chem. Mater.*, **2010**, *22*, 2190–2202.
29. D. Wang, H. L. Xin, R. Hovden, H. Wang, Y. Yu, D. A. Muller, F. J. DiSalvo and H. D. Abruña, *Nat. Mater.*, **2013**, *12*, 81–87.
30. D.-Y. Wang, H.-L. Chou, Y.-C. Lin, F.-J. Lai, C.-H. Chen, J.-F. Lee, B.-J. Hwang and C.-C. Chen, *J. Am. Chem. Soc.*, **2012**, *134*, 10011–10020.
31. X. Ji , K. T. Lee, R. Holden, L. Zhang, J. Zhang, G.A. Botton, M. Couillard and L. F. Nazar, *Nat. Chem.*, **2010**, *2*, 286–293.
32. H. Ataee-Esfahani, J. Liu, M. Hu, N. Miyamoto, S. Tominaka, K. C. W. Wu and Y. Yamauchi, *Small*, **2013**, *9*, 1047–1051.
33. M. Tian, S. Shi, Y. Shen and H. Yin, *Electrochim. Acta*, **2019**, *293*, 390–398.
34. S. Lu, K. Eid, D. Ge, J. Guo, L. Wang, H. Wang and H. Gu, *Nanoscale*, **2017**, *9*, 1033–1039.
35. L. Guo, S. Chen, L. Li and Z. Wei, *J. Power Sources*, **2014**, *247*, 360–364.
36. A. A. Belmesov, A. A. Baranov and A. V. Levchenko, *Russ. J. Electrochem*., **2018**, *54*, 493–499.
37. M. Spasojević, L. Ribić-Zelenović, M. Spasojević and T. Trišović, *Russ. J. Electrochem.*, **2019**, *55*, 1350–1359.
38. M. Spasojević, L. Ribić-Zelenović, M. Spasojević and D. Marković, *Russ. J. Electrochem.*, **2021**, *57*, 795–807.
39. M. Spasojević, L. Ribić-Zelenović and M. Spasojević, *Monatsh. Chem.*, **2021**, *152*, 489–496.
40. M. Spasojević, M. Spasojević, D. Marković and L. Ribić-Zelenović, *Z. Phys. Chem.*, **2021**, *235*, 1573–1588.
41. L. P. R. Profeti, D. Profeti and P. Olivi, *Int. J. Hydrog. Energy*, **2009**, *34*, 2747–2757.
42. T. Okanishi, Y. Katayama, R. Ito, H. Muroyama, T. Matsuia and K. Eguchi, *Phys. Chem. Chem. Phys.*, **2016**, *18*, 10109–10115.
43. B. Wang, L. Tao, Y. Cheng, F. Yang, Y. Jin, C. Zhou, H. Yu and Y. Yang, *Catalysts*., **2019**, *9*, 387.
44. A. D. Modestov, M. R. Tarasevich and H. Pu, *Electrocatalysis*, **2016**, *7*, 42–49.
45. J. González-Cobos, S. Baranton and C. Coutanceau, *J. Phys. Chem. C*, **2016**, *120*, 7155–7164.
46. Y. Liu, Y. Zeng, R. Liu, H. Wu, G. Wang and D. Cao, *Electrochim. Acta*, **2012**, *76*, 174–178.
47. K. Tran, T. Q. Nguyen, A. M. Bartrom, A. Sadiki and J. L. Haan, *Fuel Cells*, **2014**, *14*, 834–841.
48. J. L. Bott-Neto, A. C. Garcia, V. L. Oliveira, N. E. de Souza and G. Tremiliosi-Filho, *J. Electroanal. Chem.*, **2014**, *735*, 57–62.
49. B. Habibi and Dadashpour, *Electrochim. Acta*, **2013**, *88*, 157–164.
50. Y. H. Chu and Y. G. Shul, *Int. J. Hydrog. Energy*, **2010**, *35*, 11261–11270.
51. M. Wakisaka, S. Mitsui, Y. Hirose, K. Kawashima, H. Uchida and M. Watanabe, *J. Phys. Chem. B*, **2006**, *110*, 23489–23496.

52. M. A. Rigsby, W.-P. Zhou, A. Lewera, H. T. Duong, P. S. Bagus, W. Jaegermann, R. Hunger and A. Wieckowski, *J. Phys. Chem. C*, **2008**, *112*, 15595–15601.
53. P. Waszczuk, G.-Q. Lu, A. Wieckowski, C. Lu, C. Rice and R. I. Masel, *Electrochim. Acta*, **2002**, *47*, 3637–3652.
54. C. Lu, C. Rice, R. I. Masel, P. K. Babu, P. Waszczuk, H. S. Kim, E. Oldfield and A. Wieckowski, *J. Phys. Chem. B*, **2002**, *106*, 9581–9589.
55. D. R. Rolison, P. L. Hagans, K. E. Swider and J. W. Long, *Langmuir*, **1999**, *15*, 774–779.
56. J. W. Long, R. M. Stroud, K. E. Swider-Lyons and D. R. Rolison, *J. Phys. Chem. B*, **2000**, *104*, 9772–9776.
57. K. Franaszczuk and J. Sobkowski, *J. Electroanal. Chem.*, **1992**, *327*, 235–245.
58. M. D. Spasojević, N. V. Krstajić and M. M. Jakšić, *J. Mol. Catal.*, **1987**, *40*, 311–326.
59. M. Spasojević, L. Ribić-Zelenović, P. Spasojević, *Ceram. Int.*, **2012**, *38*, 5827–5833.
60. I.-S. Park, K.-S. Lee, J.-H. Choi, H.-Y. Park and Y.-E. Sung, *J. Phys. Chem. C*, **2007**, *111*, 19126–19133.